

CHAPTER 4

Chapter 4

Role of spatial and Spectral resolutions on vegetation

SUMMARY

While designing hyperspectral sensors, it becomes important to have suitable spatial and spectral resolutions as well as an idea about the dynamic range of values so that appropriate SNR can be defined. This chapter defines the optimum spectral resolutions for three broad cases of vegetation assessment -Species discrimination, Crop residue and for Phytoplanktons. The optimum spatial resolution is also defined by showing the reduction in contrast with coarsing spatial resolutions. Dynamic range of radiance is defined and based upon it the requirements for SNR are also discussed.

4.1 OPTIMUM SPECTRAL RESOLUTION

The uniqueness of hyperspectral data lies in the spectral domain-narrowness and large number. The higher spectral resolution of hyperspectral sensors compared to multispectral data enhances accuracy of vegetation related applications (Transon et al., 2018). Even with same spatial resolution, the sensor having better spectral resolution outperforms the other. This was shown by Bostan et al., 2016 where they demonstrated better performance of Hyperion over Landsat in classifying crops, while they both have a 30-m GSD. Thenkabail et al. (2004) also concluded the same for rainforest classification.

No doubt, role of optimum spectral resolution is noteworthy which is demonstrated here for discriminating vegetation species, discriminating crop residue and its management type and in identifying Phytoplanktons.

4.1.1 Method

For discriminating Crop residue using Cellulose Absorption Index (CAI)

Crop residue, when seen from space, resemble much like mature crop as well as like other farm components. Hyperspectral data can be very well used to discriminate it from other farm components. Singh et al. (2013) showed Cellulose Absorption Index (CAI) to be one of the best for this purpose. Hence, this index was used for the analyses. The Cellulose Absorption Index (CAI) is a continuum-removed spectral index in SWIR region and is based on the depth of the alcoholic C-OH absorption at 2100 nm not shared by common soil minerals thereby leading to a consistent contrast between dry residues and soils (Serbin et al, 2009). Its computation is through the following method (Daughtry et al, 2001).

$$CAI=100*(R_{2200}+R_{2000})/2-R_{2100}).....(1)$$

Spectral resolution taken from Spectroradiometer observations was degraded from 1nm to 100nm by simple averaging. CAI values were computed for all resolutions for the two group of observations, namely, crop residue discrimination and secondly for distinguishing management practices. The choice of optimum spectral resolution was done through F value check of Analysis of Variance (ANOVA).

For discriminating vegetation species using number of peaks method

Different species respond differently to different channels of the spectra because of the distinguishing constituting pigment. These pigments lead to specific peaks and troughs in the spectra. This information can be used to identify suitable bands for a specific species which can lead to species identification. Once the spectral resolution is decreased, the characteristic peaks and troughs fade away into the broader channel definition. This makes identification difficult. In order to study the same, the spectra for two classes of mangroves was taken from the Spectroradiometer observations. Each spectrum was then degraded to 10nm, 20nm, 40nm and 80nm by simple averaging technique. Following this, peak fit tool of origin Lab software was used to pick the characteristic absorption values for all the classes.

For identifying Phytoplanktons

Water attenuates the sunlight falling on it to a large extent. When ocean colour is to be studied, the surface radiance should be high enough to be recorded by the sensor. The radiance varies with the chlorophyll content. At the same time, the spectral resolution plays a significant role because the smaller spectral resolution collects more energy than finer spectral resolution. So a simulation study was carried out to observe any loss of information owing to broadening of bandwidth. Thus, a simulation study was carried out using Coupled Ocean and Atmosphere Radiative Transfer (COART) model. This tool calculates radiance and irradiance at any levels in the atmosphere and ocean. In this model, when Ocean depth is set to 0, it reduces to the conventional atmospheric radiative

transfer model. So, the model was executed by varying the bandwidths. The observations were made at solar zenith 45° when azimuth was set at 30° . The optimum spectral resolution was identified based upon the radiance profile in bandwidth broadening. The spectral resolutions studied ranged from 5nm, 10nm, 15nm and 20nm for chlorophyll setting at 0.05g/cubic metre (very low) and 5mg/cubic metre (high).

4.1.2 Results and Discussions

For discriminating Crop residue using Cellulose Absorption Index (CAI)

In the case of CAI, for all spectral resolutions and for both the groups of data, ANOVA (Figure 4.1) yielded a very low 'P' value, indicating that the classes are significantly different up to the spectral resolution of 150nm. However, the highest F value exists for spectral resolution of 10nm, thereby, indicating it to be the optimum spectral resolution for best discriminating crop residue from soil, straw and mature wheat. On looking at Figure 4.2, one finds a consistently low F value throughout but a low P value as well. This leads to the conclusion that changing spectral resolutions does not affect better identification of management practices when CAI is used.

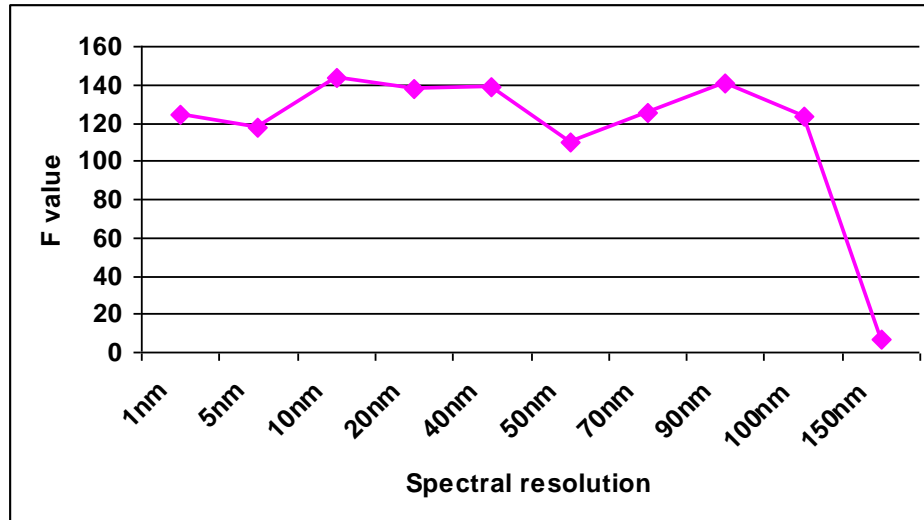


Figure 4.1: ANOVA output corresponding to CAI of visibly alike crop residue farm components for determining spectral resolution (till 150nm) beyond which crop residue discrimination become difficult

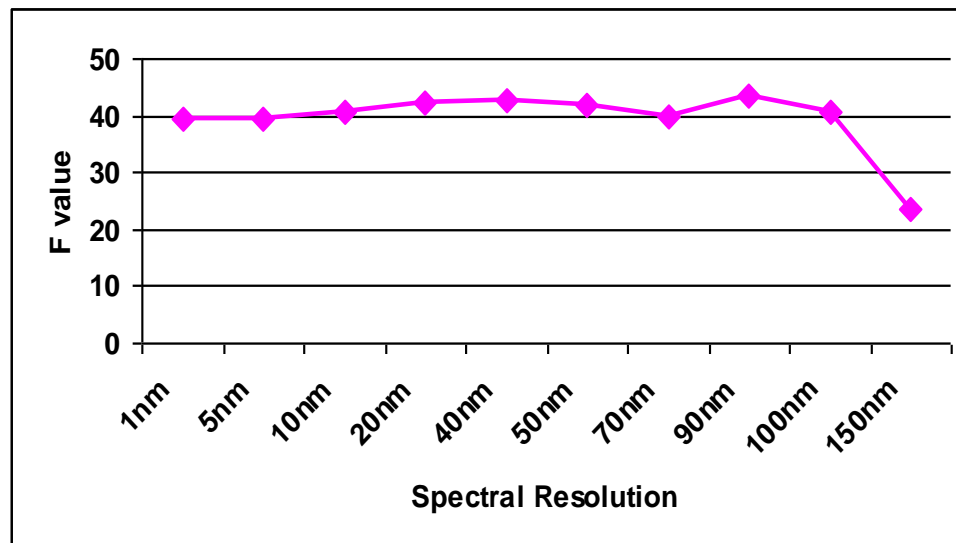


Figure 4.2: ANOVA output corresponding to CAI of different management practices for determining spectral resolution (till 150nm) beyond which crop residue discrimination become difficult

For discriminating vegetation species using number of peaks method

When two mangrove species *Avicennia marina* and *Prosopis juliflora* were investigated for the number of peaks their spectra had, the maximum number of distinguishing peaks existed for spectral resolution smaller than 10nm. Beyond 10nm, the distinguishing peaks sharply reduce and remain more or less same till spectral resolution of 80nm. This can be seen through figure 4.3. This indicates that possibility of species level classification with high accuracy is more for spectral resolution < 10nm.

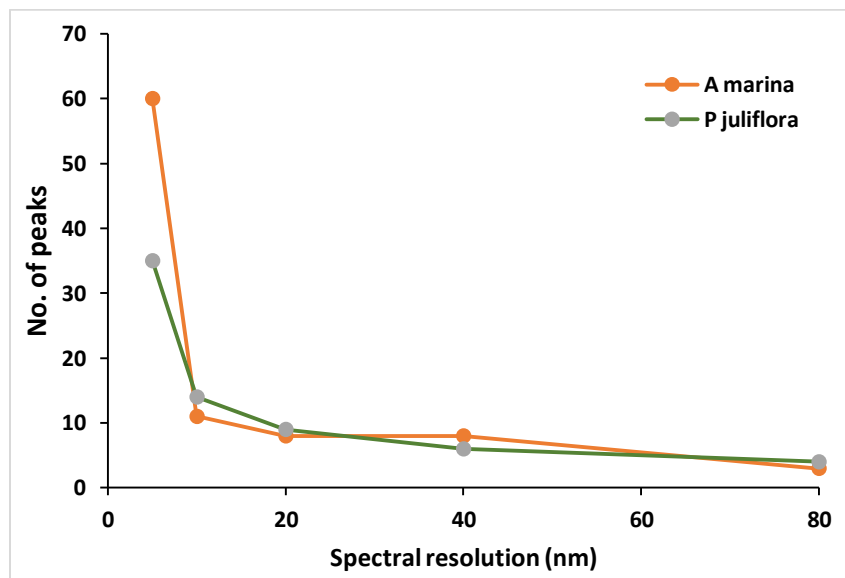


Figure 4.3: Graph showing decrease in number of peaks with coarser resolution

Considering the need for defining spectral range, when this analysis was done at 5nm, 10nm and 20nm spectral resolution, figure 4.4 is obtained. Here, at 5nm case, the maximum number of unique peaks exist (~40) within the wavelength region 1200-2500nm. At 10nm, visible through SWIR region displays unique peaks (~13) but at

20nm, the number of peaks fall to very few number (~3) and that too between 1800-2200nm. This suggests that beyond 10nm species level identification of vegetation is not possible. It is also made clear from this study that if there exists a band shift, the unique peaks would be lost.

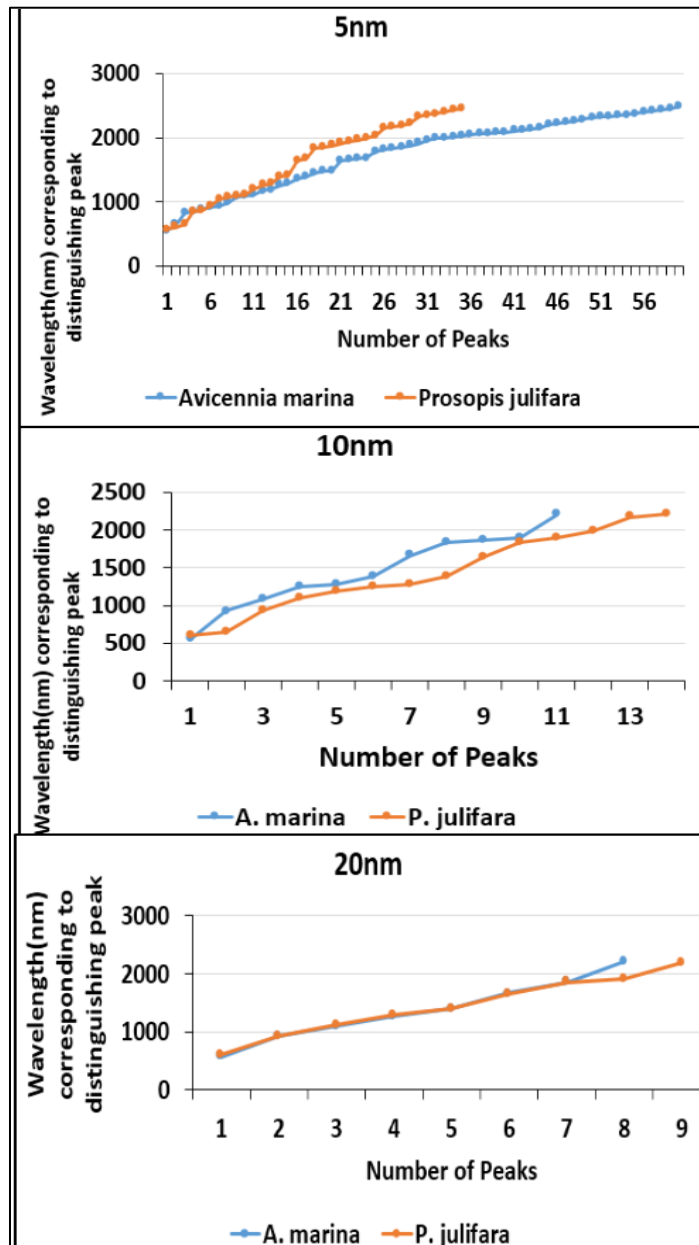


Figure 4.4: Number of Peaks at different spectral resolution corresponding to two mangrove species

Another example where effect of coarsing spectral resolution on species level discrimination is seen is presented here. Here, variation in number of distinguishing peaks on account of reducing spectral resolution for discriminating between four mangroves is seen in figure 4.5.

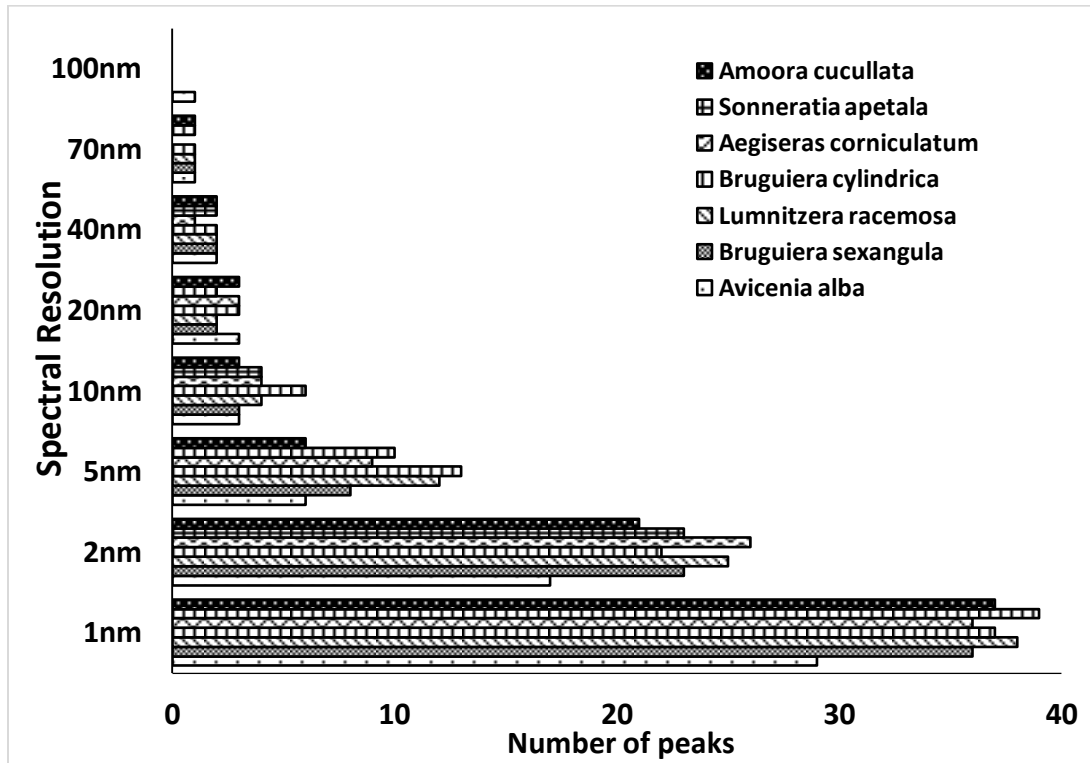


Figure 4.5: Decline in number of distinguishing peaks with reducing spectral resolution

For identifying Phytoplanktons

Radiance was simulated at 5nm, 10nm, 15nm and 20nm for sparse phytoplankton colony (chlorophyll at 0.05g/m³) and dense phytoplankton colony (chlorophyll at 5g/m³) (shown

in figures 4.6 and 4.7 respectively). In both the figures, the spectral curves flatten out at 15nm and more at 20nm. At 5nm, although lots of dips and peaks are seen yet scene noise dominates but at 10nm, the characteristic absorption points are highlighted along with very little scene noise component. Thus, 10nm spectral resolution is most suitable for the study of Phytoplanktons.

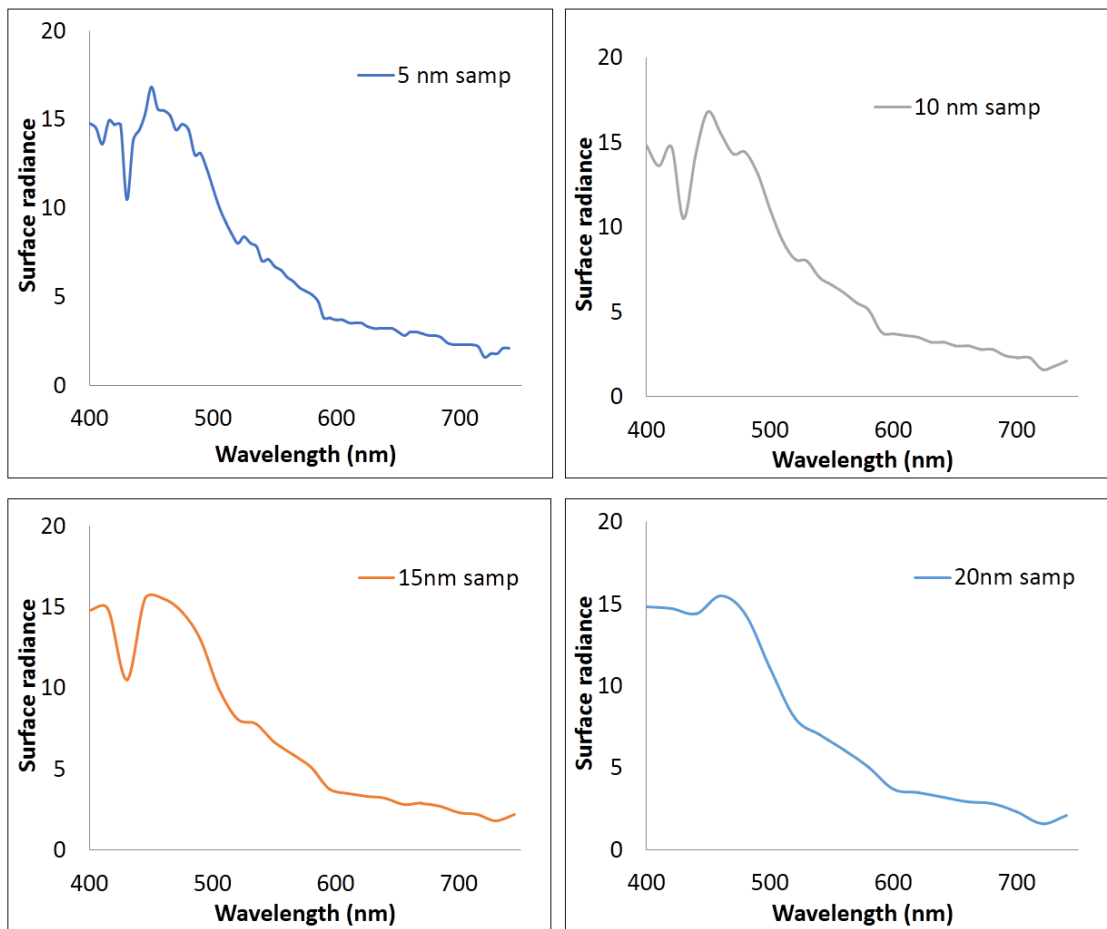


Figure 4.6: Surface radiance (mW/cm²/str/μm) at 5nm, 10nm, 15nm and 20nm from sparse phytoplankton colony

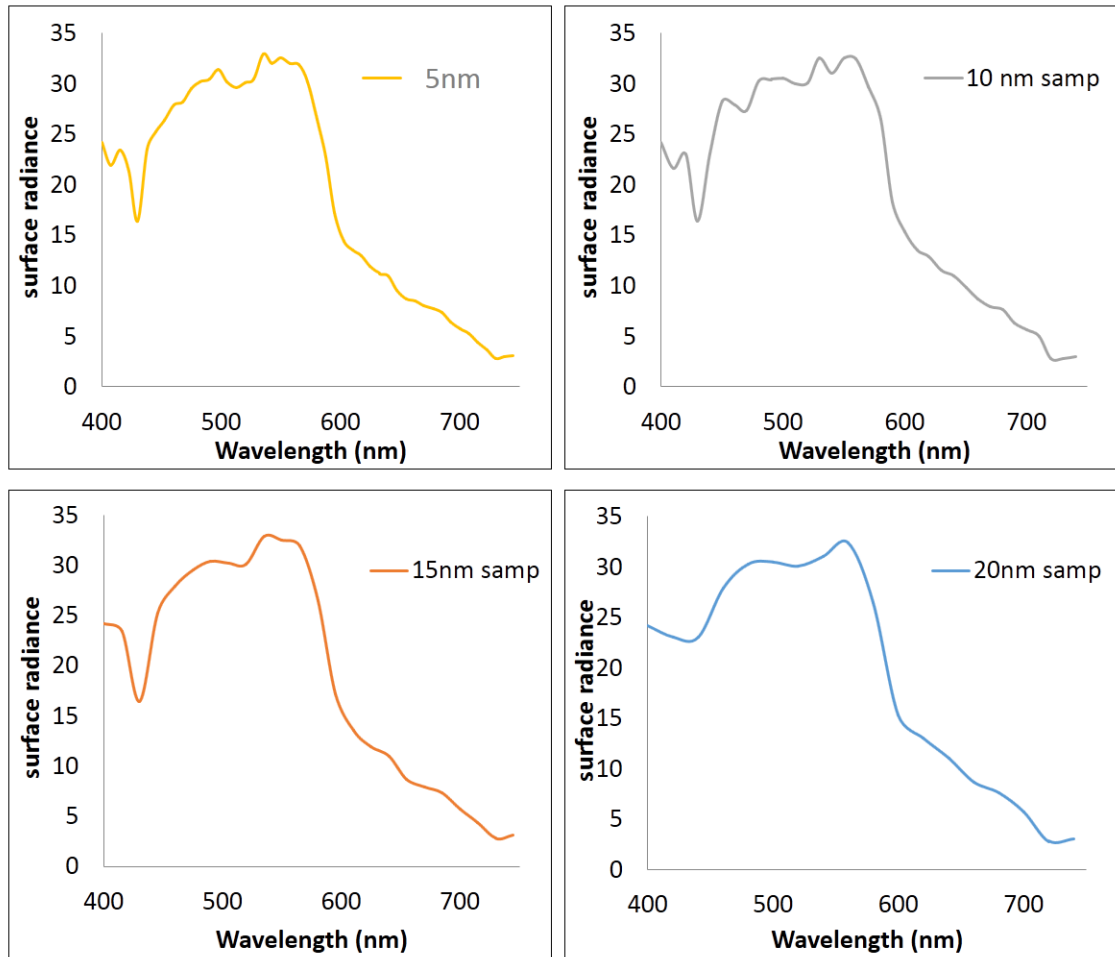


Figure 4.7: Surface radiance (mW/cm²/str/μm) at 5nm, 10nm, 15nm and 20nm from dense phytoplankton colony

4.2 EFFECT OF SPATIAL RESOLUTION

The optimum spatial resolution required to address various remote sensing studies has been one of the most crucial concerns for both the instrument designers as well as the scientists. There have been many research activities to understand the varying spatial resolution requirements for different missions for earth and planetary observations (Townshend, 1988, Curran and Willampson, 1988, Singh et al. 2002, Dadhwal, 1985,

Singh et al., 2011). Transon et al. (2018) discussed that medium spatial resolution is one of the limitation of spaceborne hyperspectral sensors because airborne hyperspectral sensors provide promising results due to high spectral resolution combined with a high spatial resolution. Thus, there is a further need to carry out similar studies helpful in identifying optimum spatial resolution for hyperspectral datasets. The effect of spatial resolution on surface characterization depends on two broad conflicting parameters viz. mixed pixels and scene noise. If the spatial resolution is decreased, the large ground resolution elements are likely to include a greater proportion of boundary information (mixed pixels) and if the spatial resolution is increased the smaller ground resolution elements are likely to pick up the finer details of the surface resulting in increased spectral overlap (scene noise). Indiscriminate refinement of spatial resolution is not advisable, as this will highlight the internal heterogeneity of the targets as well (Cushnie, 1987). The crossover in the dominance of scene noise and boundary effect occurs in the range of optimal spatial resolution which is related to the objective of the study and the scale of estimation. Spatial resolution is generally studied using the size of the target to be identified, analysis of the spatial variability and image contrast and accuracy assessment, post classification/mapping.

4.2.1 Method

As a rule of thumb, coarse resolution images have poor spatial variability then fine resolution images. Fine resolution images have sharp pixel edges or in other words show sharp contrast at the boundary line of a dark and bright object. This property is used here to identify the optimum spatial resolution. Here, original hyperspectral images (AIMS

data in this case) were spatially aggregated to coarser resolutions. It involved applying the filter with known weights (Cushnie, 1987) and resampling by half by skipping every line and every pixel. This leads to qualitative perception of the effect of spatial degradation that can be clearly seen through the images. But, for quantitative understanding, reduction in contrast (equation 2) of the images with decreasing spatial resolution were studied.

$$\text{Contrast} = (DN_{\max} - DN_{\min}) / (DN_{\max} + DN_{\min}) \dots \dots (2)$$

In contrast reduction method, the brightest (DN_{\max}) and the darkest targets (DN_{\min}) from the scene were analyzed for a number of randomly selected bands and their contrasts were evaluated. The contrasts for different resolution images were then compared with each other. The detailed approach is shown in the flow chart (Figure 4.8).

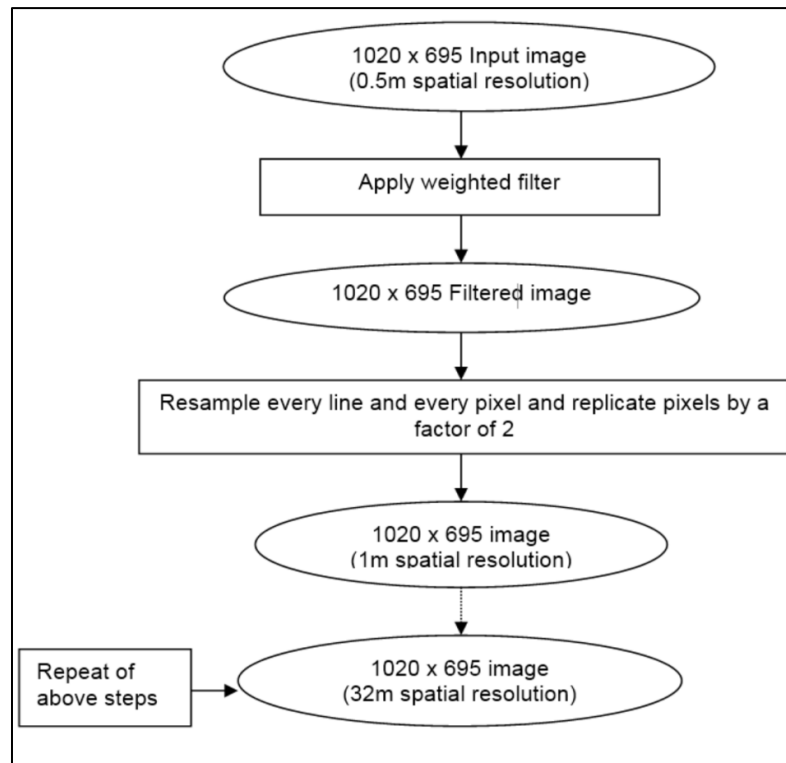


Figure 4.8: Flowchart of method of degrading spatial resolution

4.2.2 Results and Discussions

To implement the above methodology, AIMS data at 8m spatial resolution was taken. It was degraded to 16m and 32m. The effect of coarsing the resolution can be seen through figure 4.9. Visually, the effect of decreasing the spatial resolution is clear. The boundary between the pixels is increasingly getting blurred. This results in decrease in contrast.

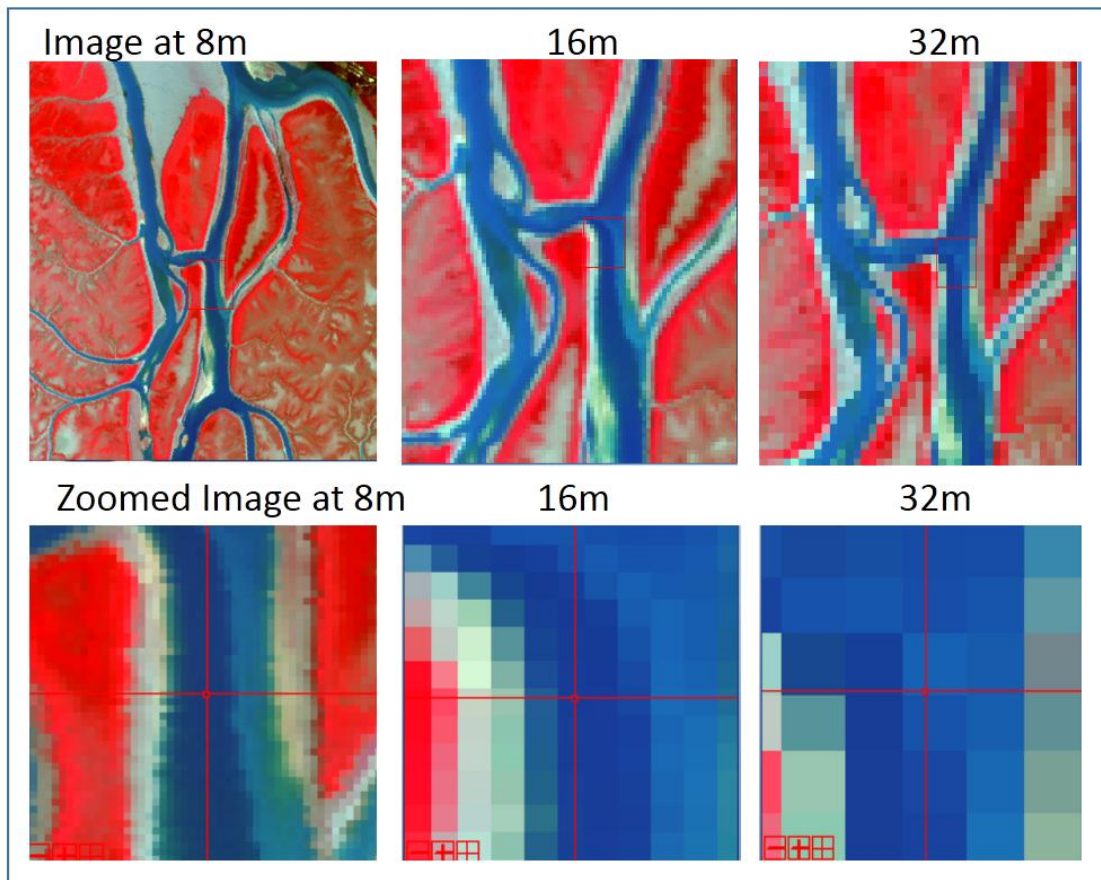


Figure 4.9: AIMS FCC at 8m, 16m and 32m spatial resolution

Thus, a quantitative analysis was needed to find the extent to which contrast decreases at each step of coarsing the spatial resolution. Contrast ratio was calculated for a large number of bands spread across the electromagnetic spectrum. Contrast ratio with

decreasing spatial resolution is plotted in figure 4.10 for bands centered at 450 nm, 550 nm, 650 nm, 750 nm, 850 nm and 900 nm.

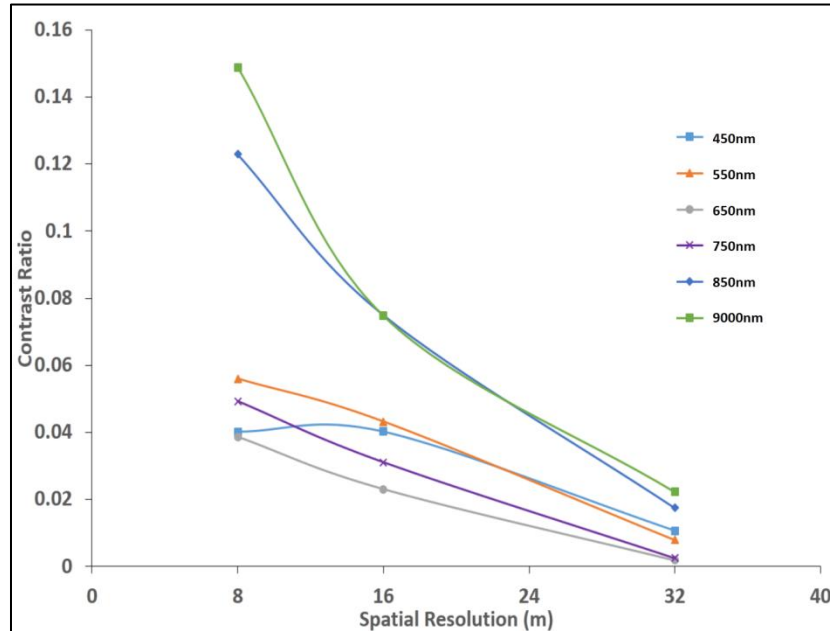


Figure 4.10: Graph showing reduction in contrast ratio as resolution becomes coarser

There is a continuous decrease in the ratio as the resolution advances indicating mixing of pixels resulting in lesser information. So, for targeting different objects different resolutions are required which depends on object size and characteristics to be retrieved. 450 nm band showed 73.14 percent reduction in contrast as compared to 94 percent reduction in case bands 550 nm, 850 nm and 900 nm while it was 95 percent for 650 nm and 94 percent for 750 nm as the resolution advances from 8.0m to 32.0m.

For spaceborne data Hyperion, the same exercise was done which yielded figure 4.11

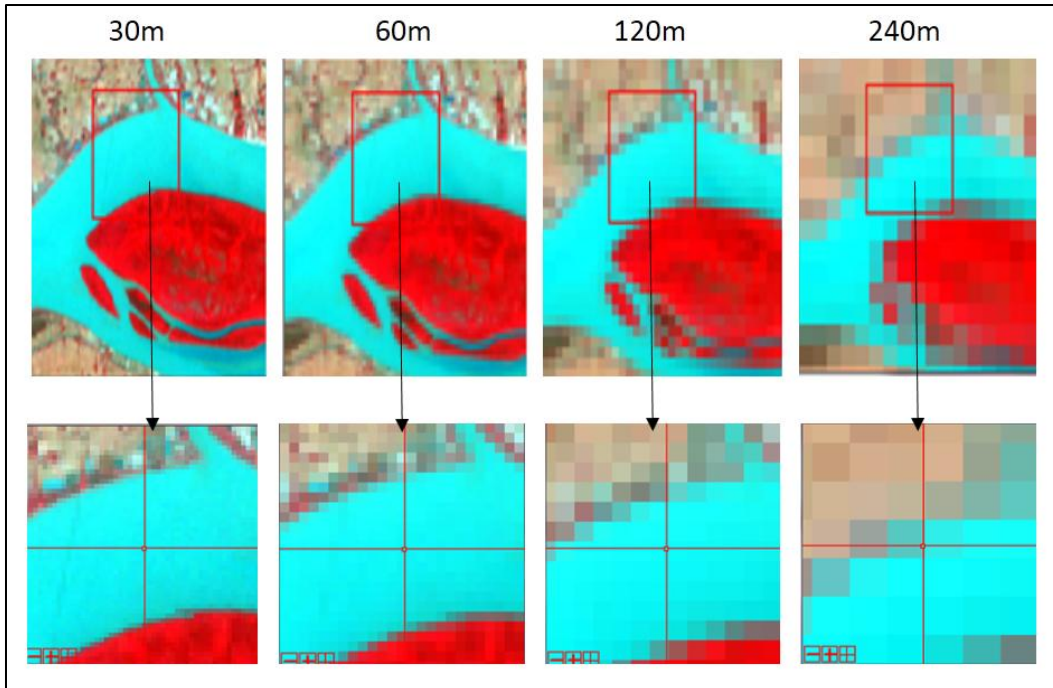


Figure 4.11: Effect of degrading spatial resolution on Hyperion data

Corresponding to the figure, reduction in contrast is shown by figure 4.12. As can be seen, contrast remains high till 60m after which it falls sharply.

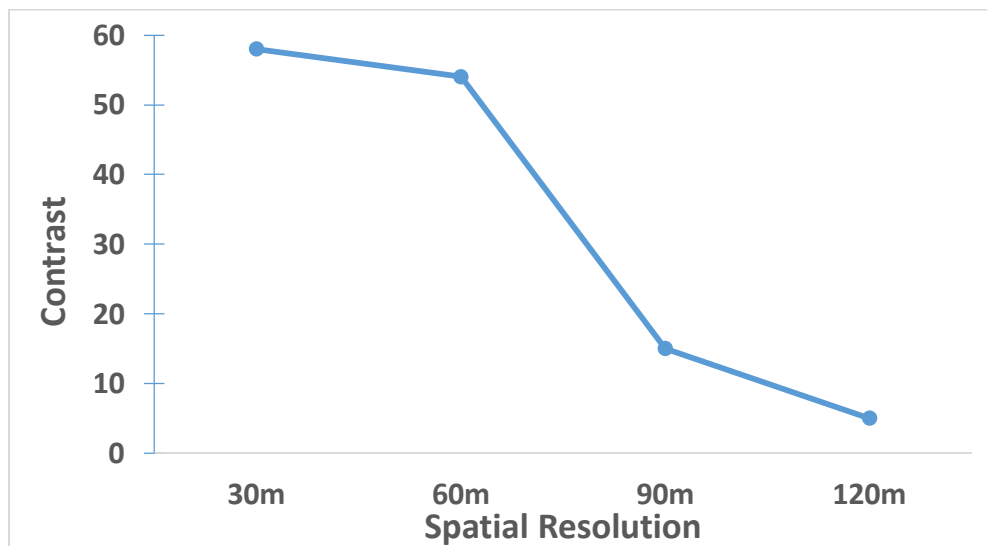


Figure 4.12: Decline in contrast ratio with decrease in spatial resolution for Hyperion

4.3 DYNAMIC RANGE AND DEFINITION OF SNR

The airborne hyperspectral instruments have a limited dynamic range and must be set to capture data over the appropriate range of signal strength. In general, the dynamic range of the instruments need to cover the darkest as well as brightest targets. There exist two types of targets-low albedo like deep water and high albedo like clouds. Vegetation comes in between the two cases. In this context, typical range of radiance values of various targets was computed. The data used for this analysis was obtained from HICO and Hyperion. Characteristically, ROI of dimension 3*3 pixels were taken for individual targets including coastal water, inland water, deep-ocean and cloud (shown in figures 4.13 and 4.14).

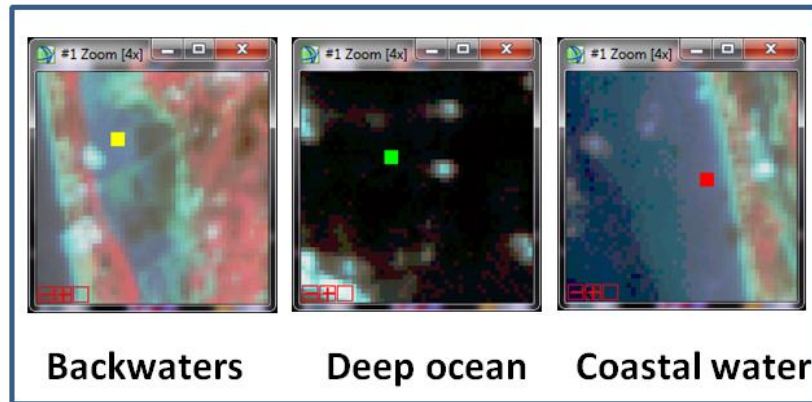


Figure 4.13: ROIs for which radiance values obtained through HICO data

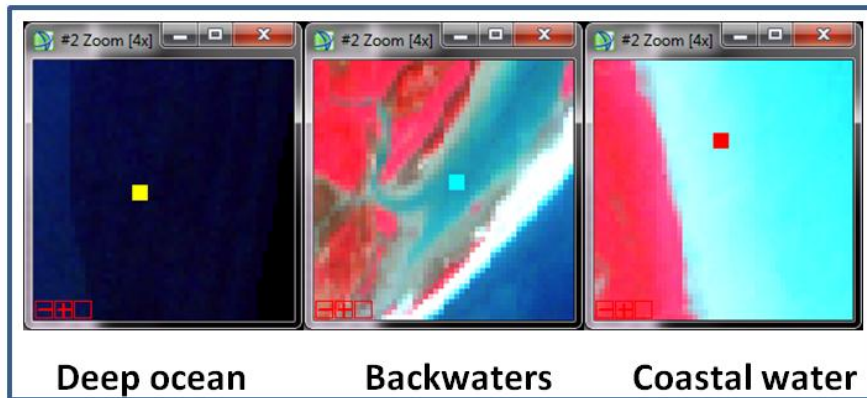


Figure 4.14: ROIs for which radiance values obtained through Hyperion data

Corresponding to these ROIs, the radiance values for the targets from HICO and Hyperion datasets are tabulated in tables 4.1 and 4.2 respectively.

Table 4.1: Radiance in $\text{mw}/\text{cm}^2/\text{sr}/\mu\text{m}$ for various targets using HICO data for selective wavelengths

wavelength (nm)	coastal water	deep ocean	clouds	backwater
375	7.1	7.6	16.3	6.8
404	7.8	7.7	24.4	7.6
427	6.8	6.5	24.8	6.4
450	7.4	6.8	31.3	7.0
473	6.8	6.0	32.0	6.3
501	5.9	4.9	31.0	5.4
524	5.4	4.1	29.9	5.4
553	4.9	3.4	29.2	5.3
576	4.3	2.8	27.6	4.6
605	3.3	2.3	26.7	3.9
627	2.9	2.0	25.3	3.2
650	2.5	1.7	24.9	3.1
673	2.3	1.6	24.8	2.6
702	1.8	1.3	22.9	3.3
725	1.3	1.0	20.3	2.5
753	1.2	0.9	18.7	2.4
776	1.2	0.9	18.7	2.4
799	1.1	0.8	18.9	2.4
828	0.9	0.7	16.8	1.8
851	1.0	0.7	17.0	1.7
874	1.0	0.7	16.5	1.6
902	0.8	0.6	14.1	1.1
925	0.7	0.6	12.0	0.8
948	0.7	0.6	9.6	0.7
977	1.0	0.8	12.9	1.0
1000	1.4	1.0	15.0	1.4
1023	1.7	1.3	16.3	1.8
1051	2.8	2.1	20.0	2.8
1080	4.9	2.6	28.9	5.3

Table 4.2: Radiance in $\text{mw}/\text{cm}^2/\text{st}/\mu\text{m}$ for various targets using Hyperion data for selective wavelengths

wavelength (nm)	coastal ocean	deep ocean	backwaters
427	6.17	5.76	5.88
529	5.79	4.63	5.17
630	5.05	2.58	3.87
722	3.36	1.29	1.87
824	2.78	0.83	1.20
925	0.75	0.25	0.36
1023	1.13	0.49	0.70
1124	0.12	0.13	0.08
1225	0.25	0.25	0.24
1326	0.12	0.10	0.10
1427	0.01	0.03	0.01
1528	0.10	0.07	0.09
1629	0.09	0.09	0.12
1730	0.07	0.05	0.06
1831	0.01	0.01	0.00
1921	0.01	0.01	0.00
2022	0.01	0.01	0.02
2123	0.01	0.01	0.02
2224	0.02	0.02	0.02
2325	0.02	0.01	0.02

It may be observed here that three bands are common in HICO and Hyperion, centered at 427nm, 925nm and 1023nm. The bands show variation in radiance values. The difference may be mainly attributed to the difference in spectral resolution which is 5.7nm for HICO and ~10nm for Hyperion, so the accumulated energy differs in both the cases. The other factors contributing to this difference in values is the difference in gain setting and the system's SNR.

As is evident from the figures above, radiance falls to below 1 mW/cm²/st/μm for Deep Ocean from ~700nm onwards while reaches a high of ~8-9 mW/cm²/st/μm for lower wavelengths. At the same time, for clouds it may reach more than 32 mW/cm²/st/μm. Hence, it would be judicious to define SNR separately for high as well as low radiance targets. Also, for low radiance targets (~0 to 1 mW/cm²/st/μm), SNR should be defined for typically three wavelength slots, as shown in table 4.3.

Table 4.3: Suggestions for SNR

Wavelength slot	Typical radiance value for deep water
1150-2500nm	<0.5 mW/cm ² /st/μm
600-900nm	2-5 mW/cm ² /st/μm
375-490nm	~5-9 mW/cm ² /st/μm

References

- Bostan, S., Ortak, M.A., Tuna, C., Akoguz, A., Sertel, E., Ustunday, B.B. (2016). Comparison of classificatyion accuracy of collocated hyperspectral and multispectral images for agricultural purposes. In Proc. of the 5th international conference on agro-geoinfo., China, pp 1-4.
- Curran, P.J., and Williamson, H.D. (1988). Selecting a spatial resolution for estimation of per-field green leaf area index. *International Journal of Remote Sensing*. 9, pp 1243-1250.
- Cushnie, J. L. (1987). The interactive effect of spatial resolution and degree of internal variability within land cover types on classification accuracies, *Int J of Remote Sensing*. 8(1), pp 15-29.
- Dadhwal, V.K. (1985). Estimation of field length, breadth and area in Vizapur (Gujarat) using Arial photographs. *Scientific Note IRS-UP/SAC/SAC/CPF/5/85*, Space Applications Centre, Ahmedabad.
- Daughtry, C.S.T. (2001). Discriminating crop residues from soil by shortwave infrared reflectance. *Agron. J*. 93, pp 125-131.
- Serbin, G., Hunt, E.R., Jr.; Daughtry, C.S.T., McCarty, G.W, Doraiswamy, P. C. (2009). An Improved ASTER Index for Remote Sensing of Crop Residue. *Remote Sensing*. 1, pp 971-991.
- Singh, R.P., Sridhar, V.N., Dadhwal, V.K, Singh, K.P, Navalgund, R. R. (2002). Comparative evaluation of Indian Remote Sensing Multi-Spectral Sensors data for crop classification. *Geocarto International*. 17(2), pp 5-9.
- Singh, Rimjhim Bhatnagar, Singh, R.P. and Ray, S.S. (2011). Mars exploration: An Information note, SAC/EPISA/ABHG/AED/IN/01/2011.
- Singh, Rimjhim Bhatnagar, Ray, S.S., Bal, S.K., Sekhon, B.S., Gill, G.S. and Panigrahy, S. (2013). Crop Residue Discrimination Using Ground-Based Hyperspectral Data. *Journal of the Indian Society of Remote Sensing*. 41(2), pp 301–308.
- Thenkabail, P.S., Enclona, E.A., Ashton, M.S., Legg, C. and De Dieu, M.F. (2004). Hyperion, IKONOS, ALI and ETM+ sensors in study of African rainforests. *Remote Sensing of Environment*. 90, pp 23-43.
- Townshend, J.R.G. (1980). The spatial resolving power of the Earth Resources satellites: A Review, NASA Technical Memorandum, 82020, National Aeronautics and Space Administration, Goddard Space Flight Centre, Greenbelt, Maryland.
- Transon, J., Andrimont, R., Maignand, A., Defourney, P. (2018). Survey of hyperspectral Earth observation applications from space in the Sentinel-2 context. *Remote sensing of Environment*. 10(2), p 157.